SEMARAK ILMU PUBLISHING

Journal of Advanced Research in Applied Sciences and Engineering Technology

Journal homepage:
https://semarakilmu.com.my/journals/index.php/applied_sciences_eng_tech/index
ISSN: 2462-1943

Development of a Higher Order Numerical Wave Tank for Internal Waves

Chelly Yi Ting Kong[1,*]

[1] Department of Civil Engineering, Universiti Teknologi PETRONAS, Malaysia

ARTICLE INFO

Article history:
Received 1 January 2026
Received in revised form 20 January 2026
Accepted 25 January 2026
Available online 9 February 2026

Keywords:

Finite difference method, arbitrary-order numerical scheme, sigma-coordinate transformation, numerical simulation, two-dimensional, velocity potential

ABSTRACT

Internal waves, particularly internal solitary waves (ISW), play a significant role in ocean dynamics and have substantial implications for offshore structures and underwater operations. The South China Sea is a region where ISW is frequently observed, posing challenges to offshore platforms, submarine navigation, and underwater infrastructure. However, accurate numerical modelling of ISW remains limited due to computational inefficiencies and a lack of publicly available simulation tools. This study presents the development of a higher-order numerical wave tank for simulating internal waves in a double-layer wave system under the rigid lid approximation. The model employs a finite difference method (FDM) combined with a sigma-coordinate transformation, enabling computations to be performed on a fixed two-dimensional grid despite spatial variations in the velocity potential, φ. An arbitrary-order stencil was implemented, allowing the numerical accuracy to be tuned according to specific real-world problem requirements. The numerical model builds upon previous work that lacked an open-source implementation. The velocity potential was solved as an intermediate step to derive the two-dimensional velocity field. With the application of the known boundary conditions, the combined-layer numerical model demonstrated satisfactory performance when validated against established benchmark test cases, with results aligning well within the understandable error margins. To further contribute to future research, the model was structured as an open source for reuse within the research group. Future development will focus on adopting second-order wave theory, removing the rigid lid approximation, and extending the model to three-dimensional configurations. These improvements bridge the gap between numerical simulations and the real-world dynamics of internal waves.

1. Introduction

Internal waves are defined as the waves that form at the interface of stratified fluids with different densities that exist in both air and marine environments. Nonlinear internal waves in the South China Sea are some of the most significant internal waves globally, with amplitudes potentially reaching 170 m [1]. Research indicates that SPAR-type floating offshore wind turbines (FOWTs) can experience surge displacements over 423 m due to the oscillating flow caused by internal waves [2]. In order to mitigate these risks, engineers need to develop numerical models that can accurately forecast the forces of the environment acting on structures by predicting the velocity potential of

* *Corresponding author.*
E-mail address: chelly_21002209@utp.edu.my

internal waves in two-fluid layer systems. As highlighted by Osborne and Burch [3], such force estimations are essential in the design of the production facilities located in the deep-water region.

Despite the growing interest in internal wave research, internal wave simulation models that are free and open source are still not available. Existing computational tools, including finite elements-based software or computational fluid dynamics (CFD) software, are not designed for internal wave simulation, and often require a license fee. An open-source implementation of a higher-order numerical wave tank model has been created to bridge this gap. The linear internal wave propagation can be simulated using this numerical model.

Before investigating the internal wave simulation, it is essential to introduce a mathematical schematic that illustrates how previous researchers have formulated the governing equations in a stratified two-layer fluid system. As shown in Fig. 1, the domain is divided into two regions, S is the lower fluid layer and S_1 is the upper fluid layer.

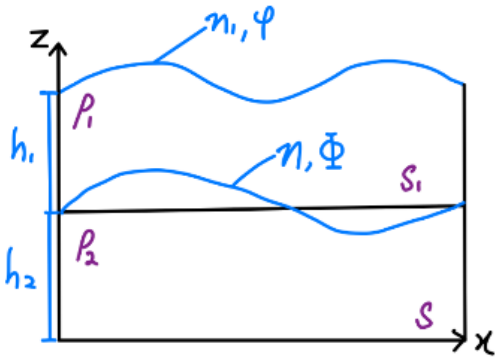

$$\Delta\Phi = 0 \; in \; the \; domain \; S(\eta) \qquad \Delta\varphi = 0 \; in \; the \; domain \; S_1(\eta_1)$$

Fig. 1. Schematic representation of the two-layer fluid system

Here, φ and Φ denote the velocity potentials for the upper and lower layers, respectively, with corresponding densities ρ_1 and ρ_2, and depths h_1 and h_2. Internal solitary waves can propagate for longer wave periods, usually about ten, and have substantially bigger amplitudes than surface waves, ranging from a few tens to several hundred meters [4]. Due to the generation of strong shear flows, their existence poses a serious threat to offshore infrastructure, drilling platforms and submarine pipelines [5,6]. Internal solitary waves can exert intense hydrodynamic forces that may cause submarines to experience sudden vertical shifts. The KRI Nanggala-402 tragedy is a well-known example, which occurred when an internal solitary wave forced the submarine past its structural depth limit [7].

Numerous numerical models have been developed for the study of internal solitary waves, each of which addresses a particular facet of wave propagation while running into different limitations. One of the earliest contributions was the Korteweg-de Vries (KdV) equation-based model, introduced by Benjamin [8], which provides a basic framework for modeling linear waves and weak nonlinear waves, but it has deficiencies in capturing large-amplitude interactions. Djordjevic and Redekopp [9] extended this framework to two-layer systems, improving internal solitary waves representation while still constrained by weak nonlinearity. The Miyata-Choi-Camassa (MCC) model developed by [10] and later refined by Choi *et al.*, [11], introduced large-amplitude wave capabilities and improved numerical stability, though it relied on the rigid-lid assumption, limiting real-world accuracy. Hao *et al.*, [12] introduced a High-Order Spectral (HOS) method with improved accuracy and numerical stability; however, its effectiveness declined in handling discontinuous density layers.

The Runge Kutta (RK) method is generally used as a numerical time marching scheme for accurate time simulation for computational fluid dynamics and wave modeling due to its ease of

implementation. The fourth-order RK method was employed to generate initial time-step data for nonlinear wave modeling over variable bathymetry [13]. This study demonstrates the necessity of implementing the fourth-order RK method for the time-marching discretization of the higher-order FDM numerical wave model. A significant issue is the lack of open-source availability. None of the reviewed researchers make their models open-source, limiting for further improvement and validation. This lack of accessibility highlights the importance of the present study.

2. Double Layer Wave Modelling

The numerical model is built on three key assumptions. To begin with, the flow is considered irrotational, indicating that as the wave moves, fluid particles travel without any rotational movement. Second, the flow is considered to be inviscid, with no viscosity. Third, a rigid lid approximation is applied, following the approach of Song [14], which considers internal wave propagation at the interface between two immiscible fluid layers of constant depth, as shown in the schematic of the two-layer fluid system below.

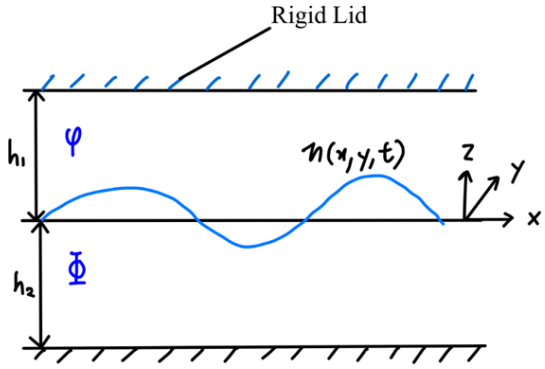

Fig. 2. Schematic of a two-layer wave model with a rigid lid

The governing equation in each layer of the combined wave modelling, introduced by Bingham *et al*., [15], is first examined. The equation is the Laplace equation with a second-order differential term, ϕ, represents the velocity potential, which is the main parameter to be solved in this model. In the equation, ϕ_{zz} represents the second partial derivative of ϕ with respect to z. The governing equation is defined as,

$$\nabla^2\phi + \phi_{zz} = 0, -h < z < \eta \qquad \textbf{(1)}$$

There are two boundary conditions applied to the interface $(z = \eta)$, including both dynamic and kinematic components. While the kinematic condition ensures that fluid particles stay at their surface during wave propagation, the dynamic condition maintains air pressure at the interface. Both the boundary conditions at the interface are defined below.

Kinematic Condition:

$$\frac{\partial \eta}{\partial t} + \frac{\partial \eta}{\partial x}\frac{\partial \phi}{\partial x}\bigg|_{z=\eta} - \frac{\partial \phi}{\partial z} = 0$$

Dynamic Condition:

$$\frac{\partial \phi}{\partial t}\bigg|_{z=\eta} + \frac{1}{2}\left[\left(\frac{\partial \phi}{\partial x}\right)^2 + \left(\frac{\partial \phi}{\partial z}\right)^2\right]_{z=\eta} + g\eta = 0 \qquad \textbf{(2)}$$

The sigma transformation method, introduced by [16] is useful in wave modelling. This method maps the physical vertical coordinate z onto a fixed sigma σ coordinate system. This approach keeps

the computational domain static and allowing the FDM to be applied at different time intervals by addressing the challenge of a moving boundary. In this study, the sigma transformation enabled a direct solution of the Laplace equation, as the vertical coordinates is redefined as,

$$\sigma(x,z,t) = \frac{z + h(x)}{\eta(x,t) + h(x)} = \frac{z + h(x)}{d(x,t)} \quad \textbf{(3)}$$

where $d(x,t) = \eta + h$ is the overall thickness of fluid layer and $h(x)$ represent the effective thickness of the wave layer, excluding the seabed variations. As a result of the sigma transformation, the Laplace equation is reformulated to

$$\nabla^2\phi + \nabla^2\sigma\phi_\sigma + 2\nabla\sigma \cdot \nabla\phi_\sigma + (\nabla\sigma \cdot \nabla\sigma + {\sigma_z}^2)\phi_{\sigma\sigma} = 0, \quad 0 < \sigma < 1 \quad \textbf{(4)}$$

All the formulas stated above will be utilized for one layer and subsequently merged into a dual-layer system by enforcing the interface boundary conditions. This study utilized an arbitrary higher-order FDM to improve numerical accuracy by utilizing a broader Taylor series expansion. Unlike the traditional second-order central finite difference approach, which uses only one forward and one backward neighboring point, the arbitrary-order higher-order FDM includes multiple neighboring points in the computation, leading to greater accuracy and stability in the numerical solution.

The analytical solution from Song [14] serves as a benchmark to validate the accuracy of the numerical model. The upper layer domain from interface to lid and the bottom layer domain span from interface to bottom, and their governing equations are defined respectively.

Upper Layer: $\Delta\varphi = 0 \quad in \quad \eta(x,y,t) \le z \le h_1$ **(5)**
Bottom Layer: $\Delta\Phi = 0 \quad in \quad -h_2 \le z \le \eta(x,y,t)$ **(6)**

The author employed the surface wave theories by Longuet-Higgins and Michael [17] and Sharma [18], in which the displacement and velocity potentials are formulated. The first-order rigid lid wave solution takes the form presented below. The formulation for the interface given by,

$$\eta_1 = \sum_{i=1}^{\infty} b_i cos(k_i x - \omega_i t + \varepsilon_i) \quad \textbf{(7)}$$

where, b_i is the amplitude. In the upper layer, the velocity potential is expressed as:

$$\varphi_1 = \sum_{i=1}^{\infty} A_i sin(k_i x - \omega_i t + \varepsilon_i), \qquad A_i = -\frac{b_i\omega_i}{k_i \sinh(k_i h_1)} \cosh[k_i(h_1 - z)] \quad \textbf{(8)}$$

In contrast, the velocity potential for bottom layer is formulated as:

$$\Phi_1 = \sum_{i=1}^{\infty} B_i sin(k_i x - \omega_i t + \varepsilon_i), \qquad B_i = \frac{b_i\omega_i}{k_i \sinh(k_i h_2)} \cosh[k_i(z + h_2)] \quad \textbf{(9)}$$

In the development of the numerical model, two boundary conditions are applied to each layer of the combined system. Using the known analytical velocity potential solution, the Dirichlet boundary condition is imposed at the shared interface between the bottom and the upper wave layers. In the bottom layer, a Neumann boundary condition is applied at the seabed to represent a no-flux condition, implying zero vertical flow through the bottom boundary. Similarly, in the upper layer, the rigid lid at the top is treated with a Neumann condition to ensure no vertical velocity. At the same time, the interface continues to use the Dirichlet condition for consistency across the layers.

3. Results and Discussion

Using a refined grid configuration with finite difference stencil order, *r = 11*, and grid dimensions $N_x = 80$ and $N_y = 78$. The results demonstrate a substantial reduction in numerical error across both layers in Fig. 3.

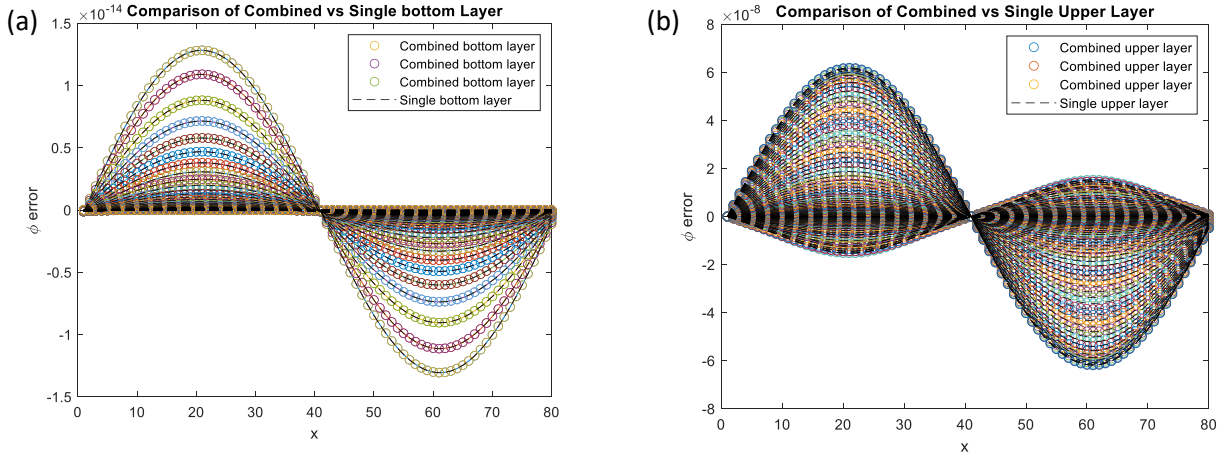

Fig. 3. (a) Comparison of single vs. combined bottom layer with refined grid (r=11, $\mathrm{N_x} = 80$, $\mathrm{N_y} = 78$), (b) comparison of single vs. combined upper layer with refined grid (r=11, $\mathrm{N_x} = 80$, $\mathrm{N_y} = 78$)

In the figures, the hollow-coloured circular markers represent the error distribution for the combined bottom and upper layers, while the black dashed line represents the single-layer formulation for both layers. As illustrated in Fig. 3, the maximum error in the bottom layer decreased to the order 10^{-14} while the upper layer error was reduced to the order of 10^{-8}. This difference between the error magnitude of the bottom and upper layers is due to the different boundary conditions applied to each layer.

3.1 Convergence Analysis with Respect to Grid Size and Stencil Order

To assess accuracy and convergence, a relative L_∞ error analysis of the velocity potential, ϕ was conducted by varying the number of vertical grid points, $\mathrm{N_y}$ and stencil order r. As shown in Fig. 4(a), the error systematically decreases with increasing grid resolution and higher-order stencil usage.

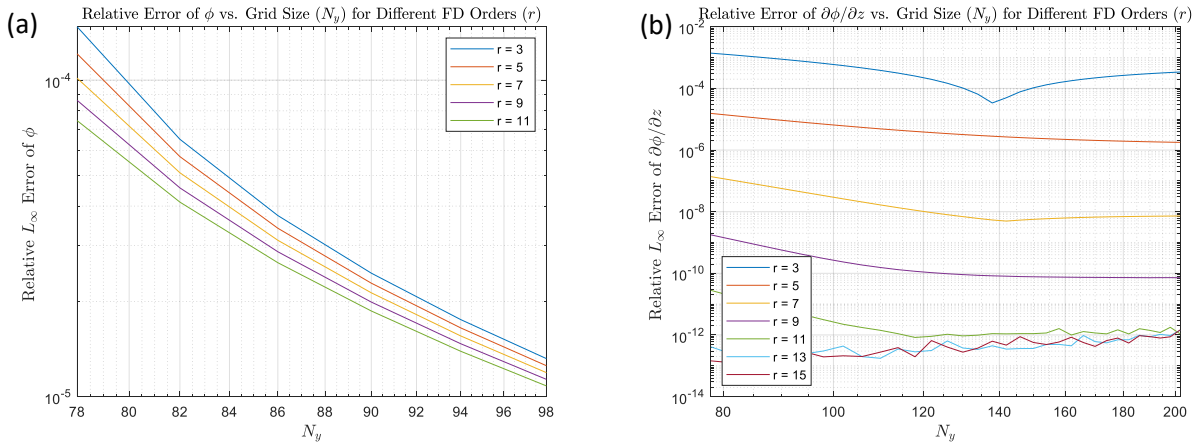

Fig. 4. (a) Log-log plot of the relative L_∞ error in the velocity potential, ϕ versus the vertical grid, N_y, (b) log-log plot of the relative L_∞ error in the vertical velocity, $\frac{\partial \phi}{\partial z}$ versus the vertical grid, N_y.

As N_y increases for a fixed stencil order, the relative error decreases, indicating consistent convergence. In addition, the accuracy of the vertical velocity component, $w = \frac{\partial \phi}{\partial z}$ of the internal wave was evaluated by computing the relative error between the FDM solution (w) and analytical solution (w_e) using the L_∞ norm. Fig. 4(b) illustrates the variation in relative errors for different FDM orders across a range of vertical grid sizes N_y. The plot of relative L_∞ norm error clearly shows that higher-order schemes combined with finer grids lead to a significant reduction in error, further confirming the precision and reliability of the developed numerical model.

3.2 Time Marching Solution for Internal Wave

The time evolution of the interface, $\eta(t)$, was computed using a fourth-order Runge–Kutta scheme for time marching. A fifth-order FDM stencil was applied, with grid dimensions of $N_x = 31$ and $N_y = 29$. The results for time variation $\eta(t)$ over two full wave periods ($T = 18s$) are presented in Fig. 5(a) and in Fig. 5(b) for the spatial distribution $\eta(x)$ along the x-direction.

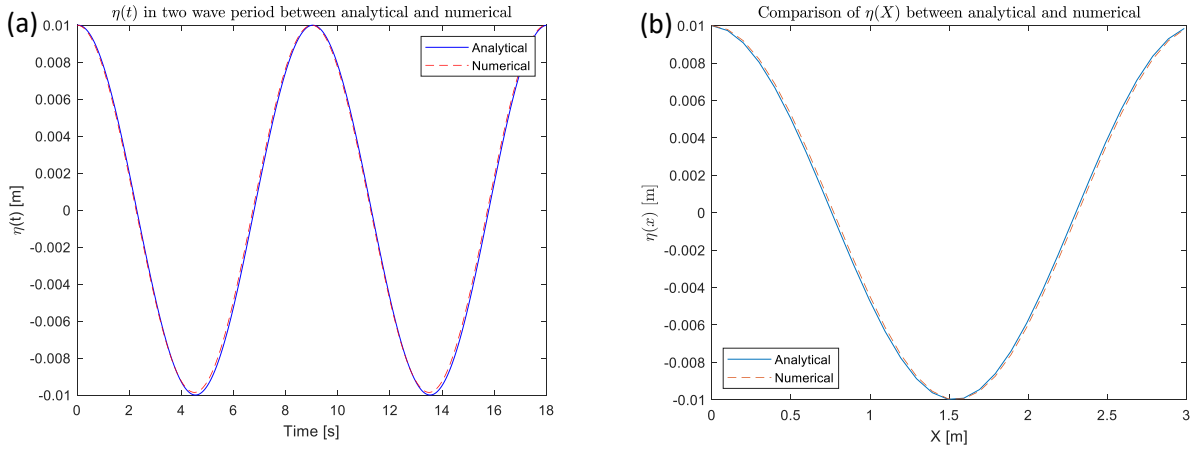

Fig. 5. (a) Comparison of $\eta(x)$ between analytical and FDM solution in two wave period, (b) comparison of $\eta(x)$ between analytical and FDM solution

The results demonstrate that the numerical model closely matches the analytical solution in both time and spatial domains. The time evolution of $\eta(t)$ confirms accurate phase alignment, while the spatial profile $\eta(x)$ along the x-direction shows strong agreement with analytical solution, confirming the precision of the fifth-order FDM stencil in capturing interface slope. The wave amplitude also aligns with the initial condition, $a = 0.01m$. Overall, the numerical model demonstrated high accuracy and stability across all the validation scenarios, verifying that this model is suitable for simulating internal wave propagation in two-layer fluid systems using arbitrary high-order finite difference methods.

4. Conclusion and Future Work

This study successfully developed a high-order numerical wave model with arbitrary schemes, allowing for the accurate estimation and propagation of linear internal waves over time in a two-layer fluid system. The numerical model is in good agreement with the analytical solution, confirming its accuracy and stability in internal wave analysis. Next, the model will be improved by removing the rigid lid approximation to include realistic free-surface interactions. Also, the framework will be extended to account for second-order nonlinear wave effects. The ultimate phase of development will aim to transition the model to a fully three-dimensional configuration, enabling more comprehensive and complex oceanographic simulations. The ultimate goal is to address the limitations in numerical modelling to bridge the gap between realistic internal wave dynamics.

Acknowledgement

The author would like to express heartfelt gratitude to the Department of Civil and Environmental Engineering, Universiti Teknologi PETRONAS, for the financial support provided under the research grant YUTP-FRG (015LC0-592).

References

[1] Klymak, Jody M., Robert Pinkel, Cho-Teng Liu, Antony K. Liu, and Laura David. "Prototypical solitons in the south china sea." *Geophysical Research Letters* 33, no. 11 (2006). https://doi.org/10.1029/2006GL025932

[2] Maertens, Vivien, Chris Blenkinsopp, and Paul Milewski. "Investigation of the influence of sinusoidal internal waves on a SPAR buoy structure." In *Journal of Physics: Conference Series*, vol. 2626, no. 1, p. 012052. IOP Publishing, 2023. https://doi.org/10.1088/1742-6596/2626/1/012052

[3] Osborne, A. R., and T. L. Burch. "Internal solitons in the Andaman Sea." *Science* 208, no. 4443 (1980): 451-460. https://doi.org/10.1126/science.208.4443.451

[4] Cai, Shuqun, Jieshuo Xie, and Jianling He. "An overview of internal solitary waves in the South China Sea." *Surveys in Geophysics* 33, no. 5 (2012): 927-943. https://doi.org/10.1007/s10712-012-9176-0

[5] Chen, Wei. "Status and challenges of Chinese deepwater oil and gas development." *Petroleum Science* 8, no. 4 (2011): 477-484. Dec. 2011. https://doi.org/10.1007/s12182-011-0171-8

[6] Pan, Zhikuan, Zhenhe Zhai, Qi Li, Qianqian Li, Lin Wu, and Lifeng Bao. "Preliminary Investigation of the Spatial-Temporal Characteristics and Vertical Dynamics of Internal Solitary Waves in the South China Sea from SWOT Data." *Journal of Marine Science and Engineering* 13, no. 2 (2025): 304. https://doi.org/10.3390/jmse13020304

[7] Gong, Yankun, Jieshuo Xie, Jiexin Xu, Zhiwu Chen, Yinghui He, and Shuqun Cai. "Oceanic internal solitary waves at the Indonesian submarine wreckage site." (2022): 109-113. https://doi.org/10.1007/s13131-021-1893-0

[8] Benjamin, T. Brooke. "Internal waves of finite amplitude and permanent form." *Journal of Fluid Mechanics* 25, no. 2 (1966): 241-270. https://doi.org/10.1017/S0022112066001630

[9] Djordjevic, V. Dj, and L. G. Redekopp. "The fission and disintegration of internal solitary waves moving over two-dimensional topography." *Journal of Physical Oceanography* 8, no. 6 (1978): 1016-1024. https://doi.org/10.1175/1520-0485(1978)008<1016:TFADOI>2.0.CO;2

[10] Miyata, Motoyasu. "An internal solitary wave of large amplitude." *La mer* 23, no. 2 (1985): 43-48. https://doi.org/10.1016/0198-0254(86)90999-4

[11] Choi, Wooyoung, and Roberto Camassa. "Weakly nonlinear internal waves in a two-fluid system." *Journal of Fluid Mechanics* 313 (1996): 83-103. https://doi.org/10.1017/S0022112096002133
[12] Hao, Xuanting, Jie Wu, Justin S. Rogers, Oliver B. Fringer, and Lian Shen. "A high-order spectral method for effective simulation of surface waves interacting with an internal wave of large amplitude." *Ocean Modelling* 173 (2022): 101996. https://doi.org/10.1016/j.ocemod.2022.101996
[13] Bateman, William JD, Chris Swan, and Paul H. Taylor. "On the efficient numerical simulation of directionally spread surface water waves." *Journal of Computational Physics* 174, no. 1 (2001): 277-305. https://doi.org/10.1006/jcph.2001.6906
[14] Song, Jin-Bao. "Second-order random wave solutions for internal waves in a two-layer fluid." *Geophysical research letters* 31, no. 15 (2004). https://doi.org/10.1029/2004GL020415
[15] Bingham, Harry B., and Haiwen Zhang. "On the accuracy of finite-difference solutions for nonlinear water waves." *Journal of Engineering Mathematics* 58, no. 1 (2007): 211-228. https://doi.org/10.1007/s10665-006-9108-4
[16] Mellor, George L., and Alan F. Blumberg. "Modeling vertical and horizontal diffusivities with the sigma coordinate system." *Monthly weather review* 113, no. 8 (1985): 1379-1383. https://doi.org/10.1175/1520-0493(1985)113<1379:MVAHDW>2.0.CO;2
[17] Longuet-Higgins, Michael S. "The effect of non-linearities on statistical distributions in the theory of sea waves." *Journal of fluid mechanics* 17, no. 3 (1963): 459-480. https://doi.org/10.1017/S0022112063001452
[18] Sharma, Jagat Narayan. *DEVELOPMENT AND EVALUATION OF A PROCEDURE FOR SIMULATING A RANDOM DIRECTIONAL SECOND-ORDER SEA SURFACE AND ASSOCIATED WAVE FORCES*. University of Delaware, 1979. https://doi.org/10.4043/3645-MS